J Digit Imaging (2012) 25:607–619
DOI 10.1007/s10278-012-9489-z

Detection of Microcalcification Clusters Using Hessian Matrix and Foveal Segmentation Method on Multiscale Analysis in Digital Mammograms

Balakumaran Thangaraju · Ila Vennila · Gowrishankar Chinnasamy

Published online: 12 May 2012

Abstract Mammography is the most efficient technique for detecting and diagnosing breast cancer. Clusters of microcalcifications have been mainly targeted as a reliable early sign of breast cancer and their earliest detection is essential to reduce the probability of mortality rate. Since the size of microcalcifications is very tiny and may be overlooked by the observing radiologist, we have developed a Computer Aided Diagnosis system for automatic and accurate cluster detection. A three-phased novel approach is presented in this paper. Firstly, regions of interest that corresponds to microcalcifications are identified. This can be achieved by analyzing the bandpass coefficients of the mammogram image. The suspicious regions are passed to the second phase, in which the nodular structured microcalcifications are detected based on eigenvalues of second order partial derivatives of the image and microcalcification pixels are segmented out by exploiting the foveal segmentation in multiscale analysis. Finally, by combining the responses coming out from the second order partial derivatives and the foveal method, potential microcalcifications are detected. The detection performance of the proposed method has been evaluated by using 370 mammograms. The detection method has a TP ratio of 97.76 % with 0.68 false positives per image. We have examined the performance of our computerized scheme using free-response operating characteristics curve.

Keywords Breast cancer · Computer Aided Diagnosis · Hessian matrix · Foveal segmentation

B. Thangaraju (✉)
Department of Electronics and Communication Engineering,
Coimbatore Institute of Technology,
Coimbatore, India
e-mail: erbala12@yahoo.com

I. Vennila
Department of Electrical and Electronics Engineering,
PSG College of Technology,
Coimbatore, India
e-mail: iven@eee.psgtech.ac.in

G. Chinnasamy
Department of Electrical and Electronics Engineering,
KSR College of Engineering,
Erode, India
e-mail: shanchinna@yahoo.com

Introduction

Breast cancer is the most common type of cancer among women and it is the second leading cause of cancer mortality. Besides skin cancer, breast cancer is the most commonly diagnosed cancer among American women [1]. According to a statistical report by the National Cancer Institute of United States, it is estimated that 230,480 women in the USA were diagnosed, out of which 39,520 women are expected to die of breast cancer in 2011 [1]. The screening mammography is the most widely used technique for detection of breast cancer. The routine screening of mammogram is evaluated as a probable option to detect the earliest signs of cancerous growth [2]. The mortality rates of women under the age of 50 have been steadily decreasing since 1990. This decrease is surmised to be the result of the advances in treatment and earlier detection through screening. Thus, early detection and adapting modern methods of treatment for breast cancer can significantly improve the survival rate of victims.

Currently, X-ray mammography is widely observed as the efficient imaging modality for early detection of abnormality. The earliest sign of breast cancer is microcalcification, which is nodular in structure with high intensity, localized or broadly diffused along the breast areas. Microcalcifications

are tiny bits of calcium deposits present in the breast tissue and they appear as clusters or in patterns associated with extra cell activity in breast region. The detection of microcalcification at an early stage is a challenging task to radiologists and a few of the clusters could not be detected by them due to their impalpable size [3]. The detection sensitivity of radiologists in microcalcification detection is 70–90 % and sensitivity depends on their experience [4]. Therefore, a Computer Aided Diagnosis (CAD) system for breast cancer detection on mammogram has been developed to improve the diagnostic rate. By incorporating the expert knowledge of radiologists, the CAD system can be made to improve the detection accuracy. Most of the researchers have proposed numerous methods based on wavelet transform, which is an efficient transform for analyzing the image hierarchically on the basis of scale. A wide range of algorithms have been proposed, intended to develop a CAD system using fuzzy logic method, artificial neural network, and genetic algorithm [5–7].

The microcalcifications appear as high frequency components in frequency domain and can be detected by frequency-based algorithm. Wang et al. have proposed an algorithm for microcalcification detection in digital mammograms based on wavelet subband decomposition [8]. In their method, detection is achieved by decomposing a mammogram into different frequency subbands, suppressing the low-frequency subband and finally reconstructing an image from the subbands containing only high frequencies. The reconstructed image contains microcalcifications additionally with some other structures, which have high frequency. Mencattini et al. [9] applied dyadic wavelet transform for enhancement of the mammogram and Nawazish et al. [10] extracted DWT features from mammogram in multiresolution analysis for detection of the suspicious areas in mammograms. Wavelet tool is effective to extract all high frequency informations, but it failed to classify the calcifications with high frequency tissues in the mammograms. Therefore, detecting only the microcalcification clusters is an important task and it can be efficiently done by introducing the structure information of microcalcifications in multiscale analysis [11].

Multiscale analysis was implemented for detection and classification of various size objects in the images. Such approaches have been developed by Frangi et al. [12], Sato et al. [13], Zhou et al. [14], and Panayiotis et al. [15]. They used Hessian matrix for vessel structures enhancement combined with multiscale analysis. Yu and Zhao [16] and Agam et al. [17] developed an algorithm to detect nodule structures on CT Images. They used Gaussian kernels of varying standard deviation for detecting local structures of images. In our CAD system, we employed a filter bank based on the Hessian matrix for distinguishing nodular structures and linear structures.

The technique that is used to find the objects of interest is referred as segmentation, which is achieved by a method called thresholding. Kom et al. [18] used local adaptive thresholding technique to segment the suspicious regions. A threshold value is calculated according to the neighborhood of the corresponding pixel and based on this threshold value, abnormal regions are segmented. Zhang and Desai [19] combined adaptive thresholding with multiresolution representation for segmentation of objects. Sahba et al. [20] used thresholding method based on fuzzy sets type II to highlight the microcalcification spots. Hu et al. [21] used probability density function with adaptive local thresholding on a multiresolution representation to segment suspicious lesions on mammograms. Existing dynamic thresholding methods did not succeed to segment the targets when objects and the background regions expressed small gray level variation. Therefore, we have used adaptive foveal thresholding method in multiscale analysis for the improvement of abnormality detection in the breast areas. The various dimensions of calcification are identified based on multiscale analysis.

Many researchers have developed a CAD system to detect calcifications based on wavelet transform, fuzzy logic, neural networks, genetic algorithm, and adaptive thresholding techniques. In their methods, the microcalcification clusters can be efficiently detected, but the tissues which appeared similar to calcifications are also detected. Therefore, the numbers of false positives are quite high in existing methods. It might be possible to reduce false positives by introducing the structure information of microcalcification into the multiscale analysis. The CAD system proposed by us has the potential to detect microcalcification clusters with high sensitivity and low false positives.

Materials and Methods

Mammogram Database

Our database consisted of 335 mammogram images having both craniocaudal (CC) and mediolateral oblique (MLO) projection view from UCSF, MIAS, and DDSM. Two hundred of them contained one or more microcalcification clusters that were annotated by radiologists, adding the total number of clusters to 242 (73 malignant lesions and 169 benign lesions), while 135 mammograms had normal images. The UCSF and MIAS database have 197 and 50 images, of which total number of microcalcification clusters is 174 (UCSF—142, MIAS—32) and the size of each mammogram is 1,024×1,024 pixels. The DDSM database was obtained from the local cancer institute with 88 images, out of which 56 were abnormal and 32 were normal. The abnormal images contain between 1 and 3 clusters per image and the total number of microcalcification clusters is 68 in DDSM database, which was previously proven by biopsy.

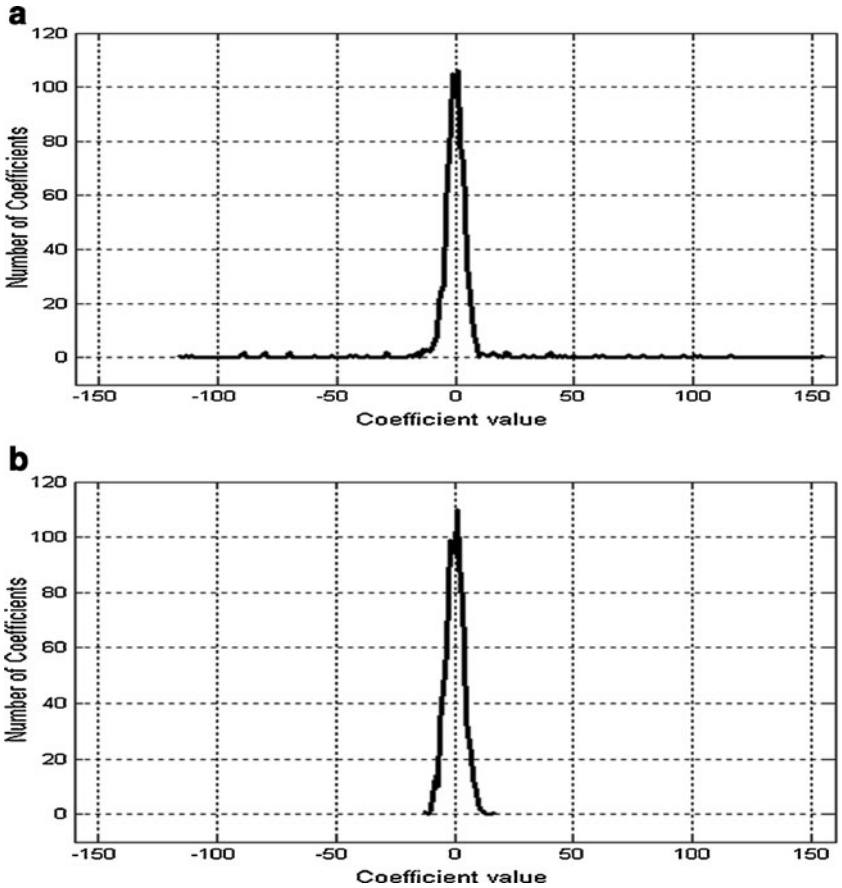

Fig. 1 **a** Cumulative histogram of region with microcalcifications. **b** Cumulative histogram of region without microcalcifications

ROI Detection

The suspicious regions in the mammograms are identified by using proposed bandfrequency based histogram technique. The bandpass image of the mammogram is used to classify the region encircling the microcalcification clusters. In order to distinguish the suspicious areas from normal areas, we performed a simulation using two data sets. The two regions with and without microcalcification clusters are selected anywhere from the bandpass frequency of the mammogram images. The size of each region is 30×30 pixels square area and histograms of both regions are determined. The cumulative histogram of

Fig. 2 ROI detection. **a** Mammogram image. **b** Suspicious regions marked on mammogram

each set is the average of the histograms of 45 regions with a microcalcification cluster and 35 regions without microcalcification cluster are shown in Fig.1(a, b). The distribution of right hand tail and left hand tail is more different in microcalcification region when compared to normal region. The difference between the end of left and right hand tail of the histogram is used to identify the suspicious regions.

The detection approach of suspicious ROI is as follows: The mammogram image is decomposed into different frequency subbands by an undecimated wavelet transform (filter bank implementation without sampling operator). The same resolution is retained at all subbands, so the size of the resulting subband images is the same as the original image. The 30×30 pixels square mask is moved on horizontal detailed subband and the difference between the maximum positive coefficient ($V_+^{\max}$) and the maximum negative coefficient ($V_-^{\max}$) is computed at each displacement.

Estimation of distance between tail end of histogram of each square region is given by

$$V_R = \left|V_+^{\max}\right| - \left|V_-^{\max}\right| \tag{1}$$

The regions in the mammogram having $|V_R| > T_h$ are identified as suspicious regions. A suitable threshold T_h has been chosen for accurate detection. A better classification is obtained while T_h is set as 6.5.

Figure 2(a) shows a mammogram image of size 2,370× 1,770 pixels with resolution of 50 μm/pixel was obtained

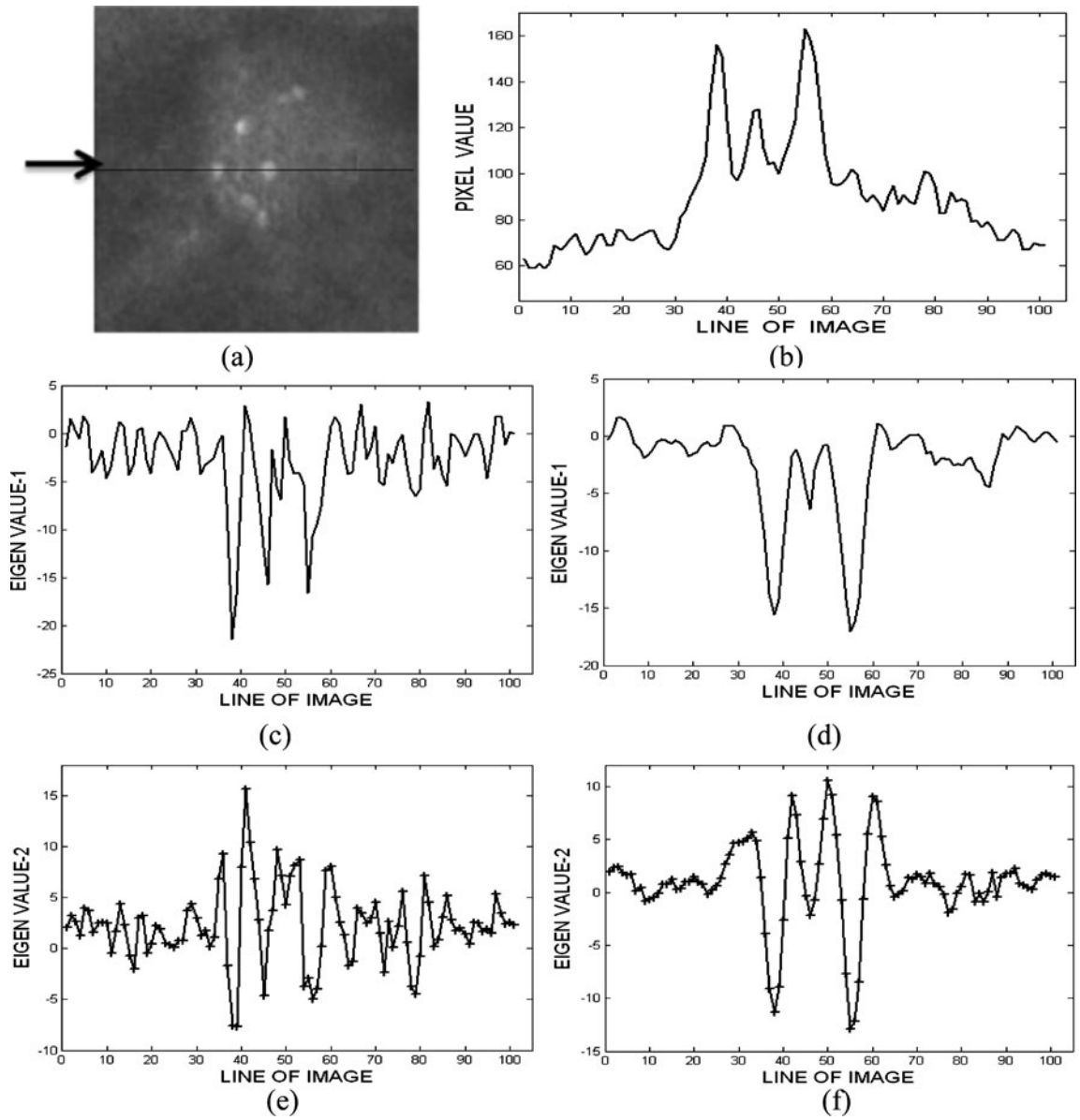

Fig. 3 **a** Region with microcalcifications clusters. **b** The line on image **c**–**d** eigenvalues-1 from scale 1 to 2 **e**–**f** eigenvalues-2 from scale 1 to 2

from Digital Database for Screening Mammography (DDSM) database. Figure 2(b) shows the suspicious regions marked by the proposed technique. It is found from Fig. 2 that the regions which do not contain microcalcifications are also marked as suspicious ROI. Therefore, the proposed approach based on eigenvalues of the Hessian matrix and foveal segmentation can significantly increase the diagnostic accuracy. A 128×128 pixels square area has been chosen as ROI size and the suspicious ROIs are extracted from the original mammogram image. The suspicious ROI contains calcifications additionally with high frequency shot noise. The shot noise is reduced by a traditional wavelet based denoising scheme [22]. In our approach, simple Donoho threshold [23] is used to suppress the noise.

Hessian Matrix

The Hessian matrix is used to identify characteristics of local shape and various structures in an image. The Hessian matrix is a square matrix and has second order partial derivates of a scalar-valued function. In the case of microcalcification detection, the function is a two-dimensional image.

The Hessian matrix is given by

$$H = \begin{bmatrix} S^{xx} & S^{xy} \\ S^{yx} & S^{yy} \end{bmatrix} \tag{2}$$

The Hessian matrix is a symmetric matrix, where the second order partial derivative S^{yx} is the same as S^{xy}.

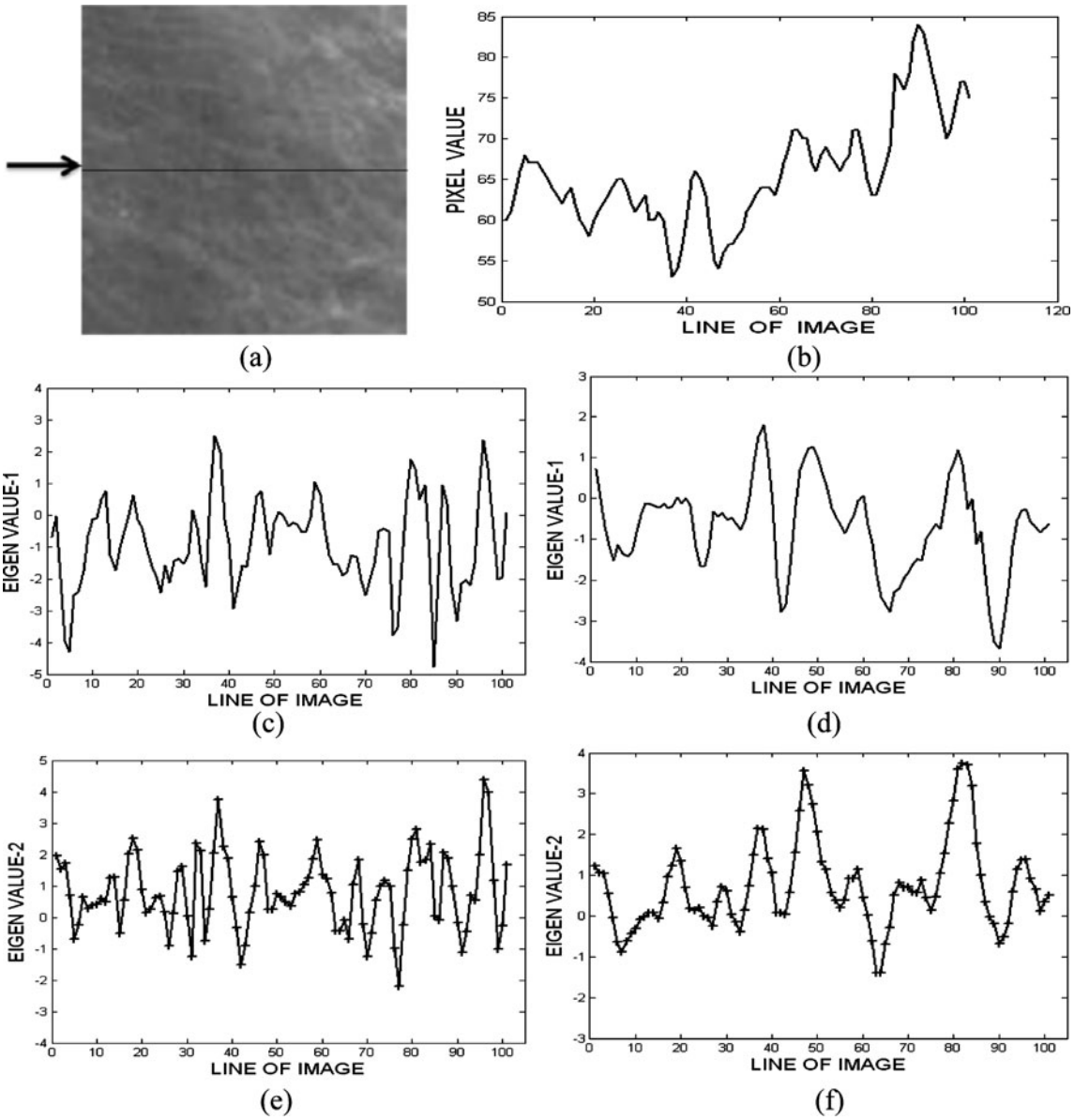

Fig. 4 **a** Region without microcalcifications clusters. **b** The line on image **c**–**d** eigenvalues-1 from scale 1 to 2 **e**–**f** eigenvalues-2 from scale 1 to 2

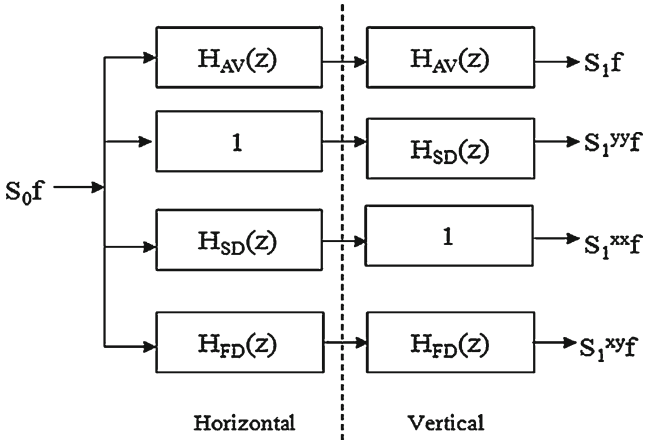

Fig. 5 Filter bank for computing eigenvalues of Hessian matrix

Therefore, the computation complexity of Hessian matrix is reduced by using this property. The partial derivatives are expressed as intensity variation in horizontal and vertical directions.

The second order partial derivative of image S is computed by

$$\frac{\partial}{\partial x}\left[\frac{\partial S}{\partial x}\right] = S^{xx}, \frac{\partial}{\partial y}\left[\frac{\partial S}{\partial y}\right] = S^{yy}, \frac{\partial}{\partial x}\left[\frac{\partial S}{\partial y}\right] = S^{xy} = S^{yx} \quad (3)$$

The eigenvalues of the Hessian matrix provide the structure information of the image and these values state the local intensity variation in the direction of the associated eigenvectors v_1 and v_2. The associated eigenvalues are λ_1 and λ_2 with $|\lambda_1| > |\lambda_2|$

The eigenvalues are computed by

$$v_1^T H v_2 = diag[\lambda_1, \lambda_2] \quad (4)$$

The multiscale analysis is used to identify small and large size calcifications in the mammogram. In order to study the relation between eigenvalues of the Hessian matrix with different structures of the image in multiscale analysis, we selected two regions from the mammogram and simulated. A single row on the mammogram image was taken, which contained microcalcifications. Figure 3 shows that the line of image contains two sharp peaks which indicate microcalcification cluster and other samples which indicate background information. Multiscale analysis was applied to the line of image, where scale increases and the magnitude of eigenvalues at calcifications reduce, but it is not less than zero. Figure 3(c–f) show eigenvalues of the Hessian matrix for this line at different scale. However, the eigenvalues at edges of the calcifications are positive values and at the center are large negative values. The eigenvalues of background informations are random values where scale increases the values close to zero.

The other line which does not contain calcifications was selected randomly in the mammogram is shown in Fig. 4. The two eigenvalues for this line are small random values and do not have large negative values in each scales. Therefore, microcalcification clusters can be detected accurately by using eigenvalues of the Hessian matrix.

The various sizes of microcalcifications can be detected by using multiscale approach. Panayiotis et al. [15] used Gaussian kernel as smoothing function and here we have proposed smoothing filter with filter bank based on Hessian matrix for

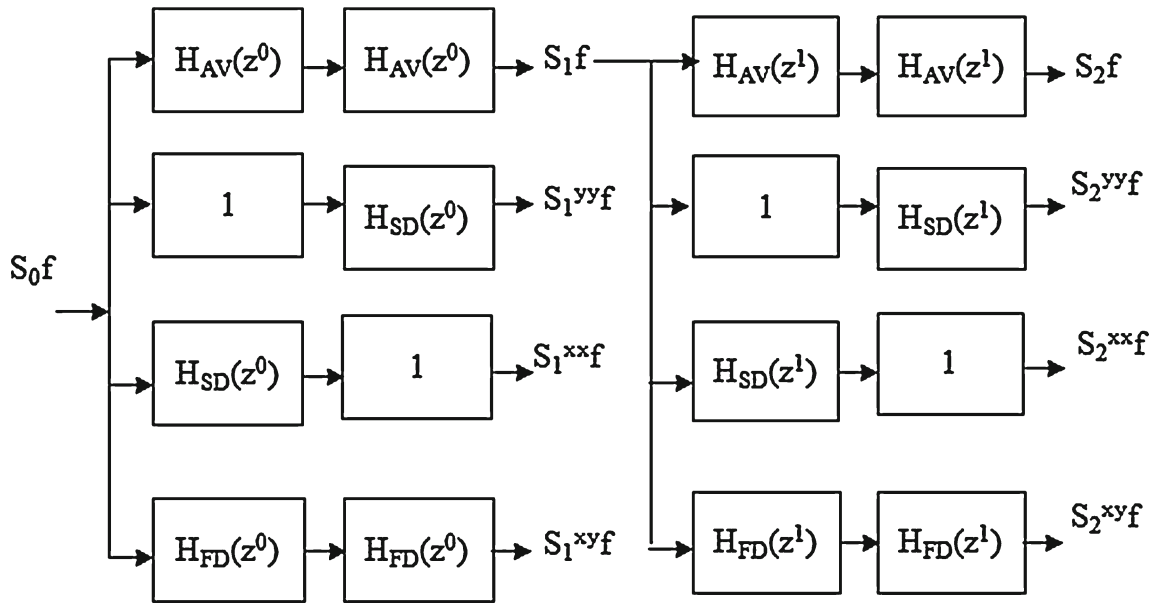

Fig. 6 Filter bank obtained by iterating the smoothing response

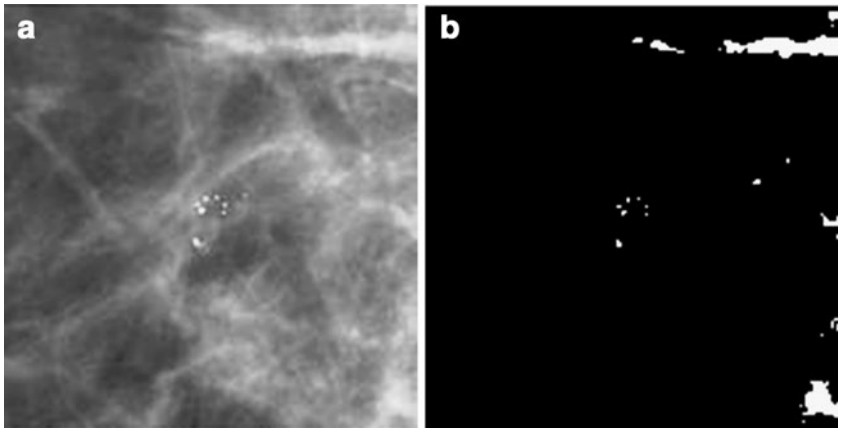

Fig. 7 **a** Part of mammogram. **b** Bithresholded image

multiscale analysis. The unwanted artifacts and background noise are suppressed when the image gets smoother.

The first order and second order partial derivatives of a function $f(x)$ are given by

$$\frac{\partial f}{\partial x} = \frac{1}{2}(f(x+1) - f(x)) \tag{5}$$

$$\frac{\partial^2 f}{\partial x^2} = \frac{1}{4}(f(x+1) + f(x-1) - 2f(x)) \tag{6}$$

The z transform of these derivatives are given by

$$\mathrm{HFD(z)} = \frac{1}{2}\left(z^1 - 1\right) \tag{7}$$

$$\mathrm{HSD(z)} = \frac{1}{4}\left(z^1 + z^{-1} - 2\right) \tag{8}$$

Let H be the Hessian matrix from Eq. (2), the Hessian matrix expresses the second order intensity variation around the pixel [24]. The S^{xx} and S^{yy} are second order partial derivatives in horizontal (rowwise) and vertical (columnwise) direction, S^{xy} is first order derivative in horizontal followed by vertical direction. Smoothing filter is an averaging filter which is used to blur the image and weaken high frequency structures. The smoothing filter reduces the sharp intensity variation in the image. This filter is also referred to as approximation filter.

We employed the second order averaging filter

$$\mathrm{H_{AV}(z)} = \frac{1}{4}\left(z^1 + z^{-1} + 2\right) \tag{9}$$

The response obtained by the smoothing filter is the average value of the immediate neighborhood of the pixel.

Figure 5 shows a filter bank which is designed based on Hessian matrix. S_0f is an original image, the smoothed image (S_1f) is obtained by applying second order average filter in the horizontal direction followed by vertical, $S_1{}^{yy}f$ is obtained by applying second order derivative filter in vertical direction, $S_1{}^{xx}f$ is obtained by applying second order derivative filter in horizontal direction and $S_1{}^{xy}f$ is obtained by applying first order derivative filter in horizontal direction then in vertical direction. $S_1{}^{yx}$ is same as $S_1{}^{xy}$, therefore it is not necessary to compute $S_1{}^{yx}$ using filter.

The multiscale representation is achieved by iterating the smoothed image according to Fig. 6. The image gets smoothened and the details in the image are suppressed at each scale. The 2^j is usually utilized for the order of z at scale j in order to obtain more detailed information at each scale. The filter $H_{\mathrm{AV}}(z^j)$, $H_{\mathrm{SD}}(z^j)$, and $H_{\mathrm{FD}}(z^j)$ is the 2^j scale dilation of $H_{\mathrm{AV}}(z^0)$, $H_{\mathrm{SD}}(z^0)$, and $H_{\mathrm{FD}}(z^0)$. The 2^j scale dilation means placing (2^j-1) zeros between the original coefficients. The original coefficients are computed according to Eqs. (7, 8, and 9). If the size of the input image S_0f is $M\times N$ pixels then smooth image at each scale (2^j) retains the same size.

The eigenvalues of the Hessian matrix for each pixel of an image at different scale are computed, the

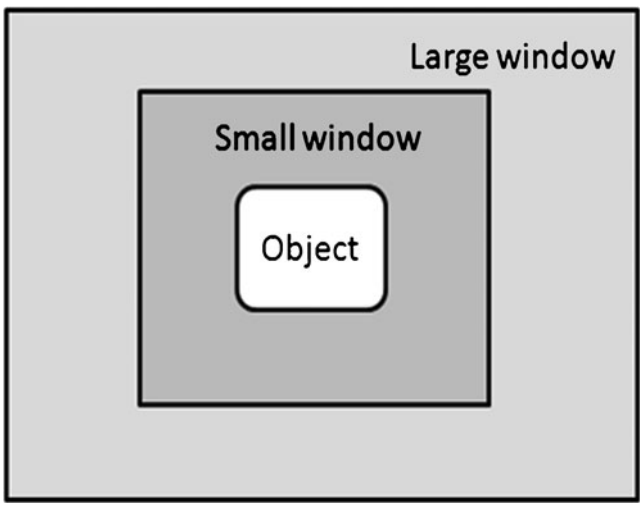

Fig. 8 Windows for foveal segmentation

abnormalities are identified according to the following decision rule:

$$H_j^D(x,y) = \begin{cases} 1 & \lambda_{1,j}^{x,y} < Nv,\ \lambda_{2,j}^{x,y} < 0 \\ 0 & otherwise \end{cases} \quad (10)$$

In this rule, H_j^D is a resultant binary image, $\lambda_{1,j}^{x,y}$, $\lambda_{2,j}^{x,y}$ are the eigenvalues of the Hessian matrix of pixel coordinate (x,y) at scale j. Nakayama et al. [11] used the condition λ_1, $\lambda_2<0$ in multiresolution representation for detection of the microcalcification nodules. Their method additionally detects unwanted high frequency nodules. It is found from Fig. 3(c–f), the eigenvalues at calcifications are decreased (negatively) in every scale. Therefore, N_v value is varied at each scale for improving diagnostic accuracy. We have found from various experiments that the optimal value N_v=−4 (Scale 1) provides the best detection results. At each scale, $|N_v|$ value is decreased by one. The areas having λ_1, λ_2 satisfy the above conditions and are marked as suspicious areas.

Proposed Algorithm with Foveal Segmentation

Thresholding is the one of the obvious methods to segment the target objects from the image. Figure 7(a) shows a part

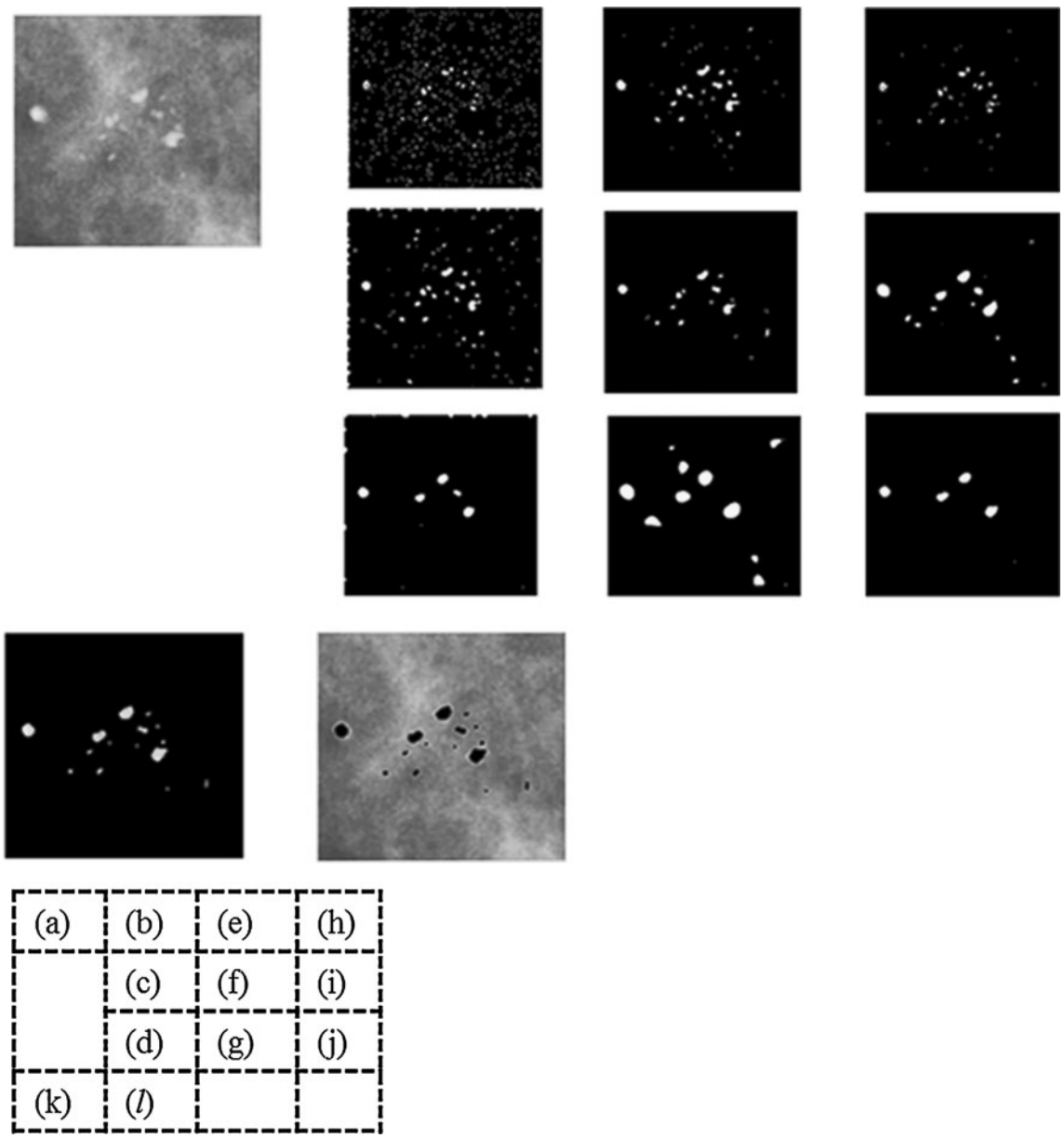

Fig. 9 **a** Suspicious region image. **b**–**d** Binary results obtained by eigenvalues of Hessian matrix. **e**–**g** Binary results obtained by foveal algorithm. **h**–**j** Combined results. **k** Final resultant image. **l** Resultant image indication on mammogram image

of the mammogram image with microcalcification clusters and Fig. 7(b) shows the binary threshold of the same image. It is easier to distinguish target objects against dark background rather than light background. The visual perception of tiny objects over denser background is even more difficult because objects are embedded with a neighborhood of objects. The global threshold technique is used to segment the objects against their background. But the determination of the threshold value is complex to the threshold-based algorithms. The clusters of microcalcification appear in the mammogram as bright spots and almost 5 % of the pixels cover the entire microcalcification clusters in the mammogram image. We used dynamic threshold technique instead of global threshold to improve the efficiency of microcalcification detection. Linguraru et al. [25] proposed foveal segmentation for microcalcification detection. We have slightly modified their algorithm, so that the modified algorithm detects different sizes of calcifications present in the mammogram. We have proposed multiscale based foveal segmentation for achieving high detection sensitivity.

The algorithm comprises the following steps. The set of average pixel intensities of object window (μ_0), its small window neighborhood (μ_{SW}), and large window neighborhood (μ_{LW}) are computed according to Fig. 8. The average pixel intensity of the small window neighborhood (μ_{SW}) is calculated from pixels within the small window excluding the object and the large window pixels. Similarly, average pixel intensity of the large window neighborhood (μ_{LW}) is

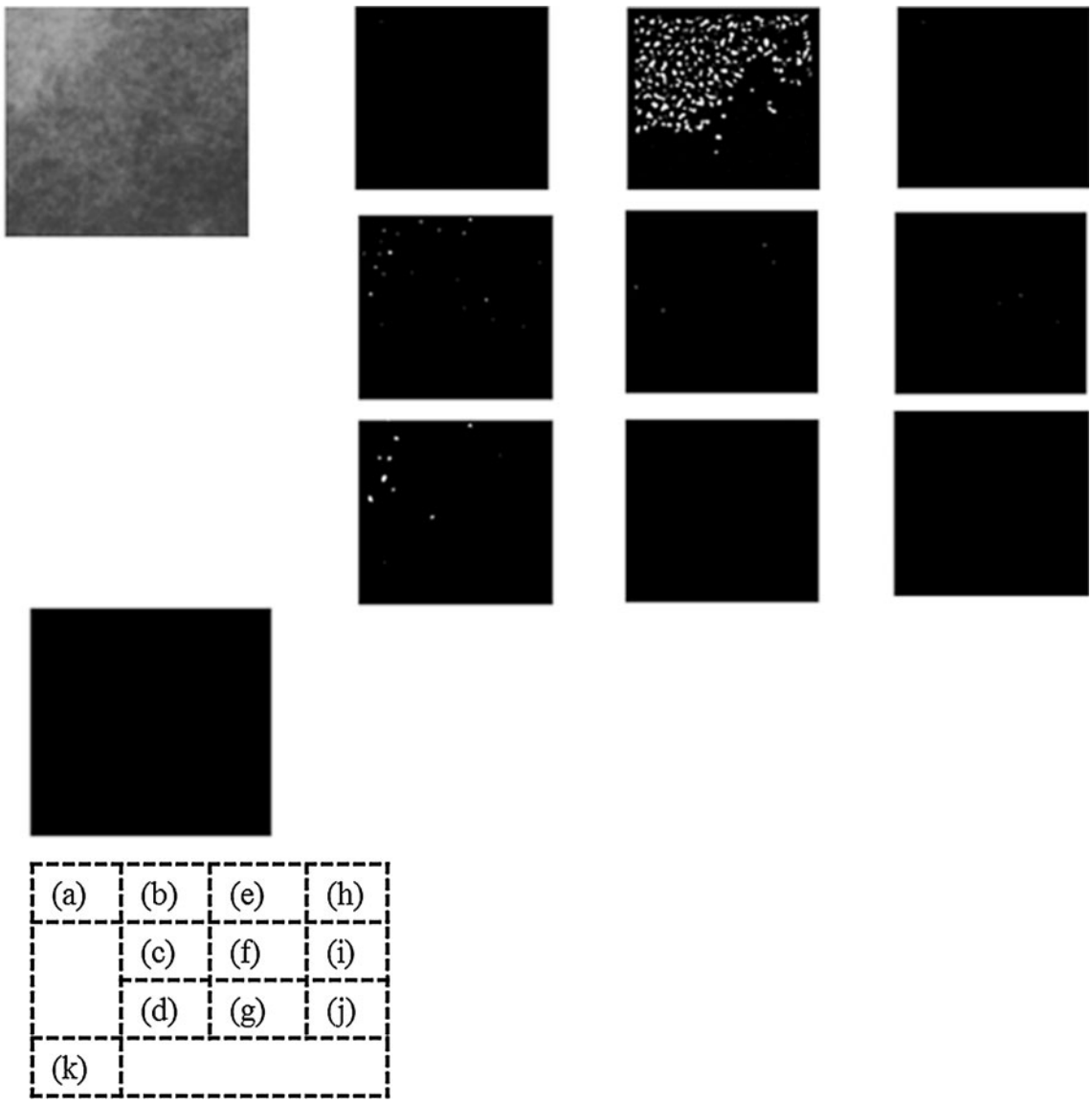

Fig. 10 **a** Normal region image. **b**–**d** Binary results obtained by eigenvalues of Hessian matrix. **e**–**g** Binary results obtained by foveal algorithm. **h**–**j** Combined results. **k** Final resultant image

Table 1 TPs and FPs detected by the proposed method

Database	Number of images	Number of abnormal images	Number of normal images	Number of clusters	TP detected	Number of FPs from entire images	TP ratio % with FPs
MIAS Database	50	27	23	32	31	24	96.87 % with 0.48 FPs
UCSF	197	117	80	142	140	144	98.59 % with 0.73 FPs
DDSM with 50 μm/pixel	88	56	32	68	66	68	97.05 % with 0.77 FPs
Total images	335	200	135	242	237	236	97.93 % with 0.70 FPs

calculated within large window only except the pixels of object, small window and background. The size of the small window is double the size of the object window and the large window size is thrice the size of the object window.

The microcalcifications appear as subtle bright spots of sizes between 0.6 and 2 mm in the digital mammograms. Therefore, initial object kernel size is a 5×5 pixels square matrix, which is sufficient to detect the small microcalcifications in the mammogram. The object window size is incremented by one at each scale for the detection of diverse size microcalcifications accurately. In Lingaguru et al. [25] method, the kernel size of the object is constant for all mammogram images.

Perceivable contrast of a pixel is computed by

$$C_p(x,y) = \begin{cases} \mu_0 - \mu_{SW} & \mu_0 > \mu_{SW} \\ 0 & Otherwise \end{cases} \quad (11)$$

μ_0 is average pixel intensity value of object window centered at pixel coordinate (x,y) and μ_{SW} is average pixel intensity value within the small neighborhood except the pixels in the object window. The pixel that has perceivable contrast is greater than adaptive threshold and is identified as microcalcification pixel.

The adaptive threshold $T_H(x,y)$ is calculated by

$$T_H(x,y) = \begin{cases} (0.808 + K)^2 & \mu_{LW} > \mu_{SW} \\ \left(0.808 + \frac{\mu_{SW}}{K}\right)^2 & \mu_{SW} > \mu_{LW} \end{cases} \quad (12)$$

where $K = \sqrt{0.923\mu_{SW} + 0.077\mu_{LW}}$ is found from literature [26], which is used to reduce false positives in the mammogram.

Let binary image F be the segmentation result

$$F(x,y) = \begin{cases} 1 & C_p(x,y) \geq \lambda . T_H(x,y) \\ 0 & otherwise \end{cases} \quad (13)$$

where λ is a bias thresholding constant with its value between zero and one. We found by trial and error basis that $\lambda = \frac{\sqrt{\sigma(S^{yy}f)}}{140}$ gives good detection of microcalcification, where $\sigma(S^{yy}f)$ is the standard deviation of second order partial derivative of the corresponding image.

The above segmentation method is combined with the multiscale analysis that allows for finding various sizes of microcalcifications. In the previous section, we have developed a

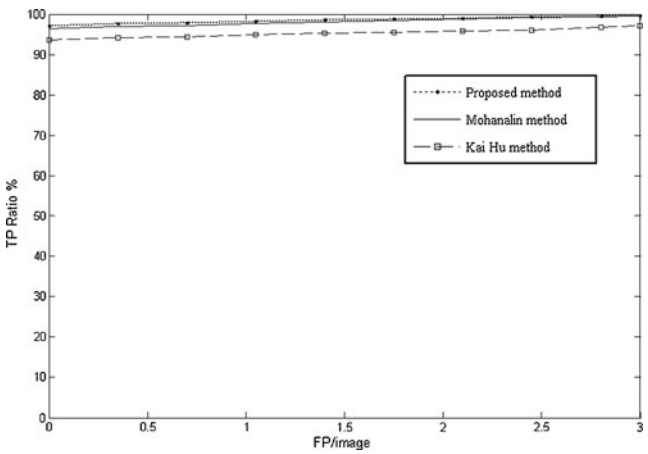

Fig. 11 The comparative FROC curves for microcalcifications detection. The clusters were selected from UCSF, MIAS, and DDSM database with resolution of 50 μm/pixel

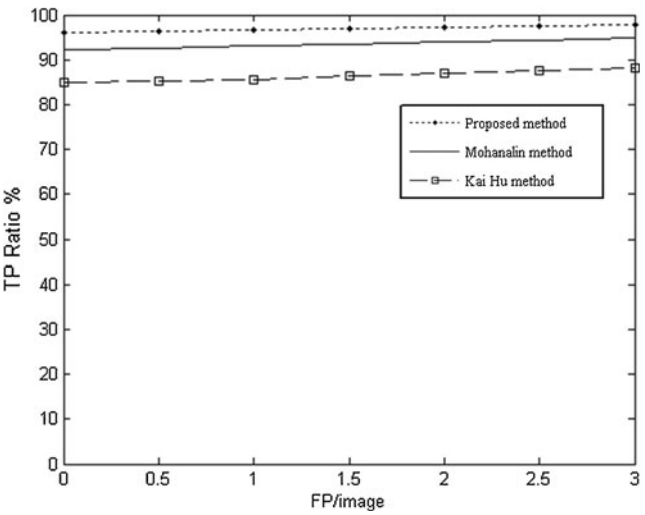

Fig. 12 The comparative FROC curves for microcalcifications detection. The clusters were selected from DDSM database with resolution of 42 μm/pixel

Table 2 TPs and FPs detected by the proposed method

Database	Number of images	Number of abnormal images	Number of normal images	Number of clusters	TP detected	Number of FPs from entire images	TP ratio % with FPs
MIAS Database + UCSF + DDSM with 50 μm/pixel	335	200	135	242	237	236	97.93 % with 0.70 FPs
DDSM with 42 μm/pixel	35	24	11	27	26	18	96.29 % with 0.51 FPs
Total images	370	224	146	269	263	254	97.76 % with 0.68 FPs

filter bank based on multiscale analysis. The foveal segmentation method is applied to the approximation image (S_jf) and the suspicious pixels are marked at each scale according to Eq. (13). The set of binary images are obtained by using both Hessian matrix and foveal segmentation in multiscale analysis.

We proposed the following condition for achieving microcalcification detection

$$M_j(x,y) = \begin{cases} S(x,y) & H_j^D(x,y) = 1,\ F_j(x,y) = 1 \\ 0 & otherwise \end{cases} \quad (14)$$

S is an original mammogram image; H_j^D and F_j are binary images at scale j obtained by Eqs. (10) and (13). We combined the response (M_j) obtained by the multiscale filter at different scales to obtain a final detection of microcalcification which is

$$M_{\text{det}} = \max\left(M_j\right)_{1\le j\le J} \quad (15)$$

In this rule, J is the maximum scale, which can be chosen to detect large size calcifications. We performed experimental tests on 242 suspicious ROIs with microcalcification cluster. We have found from the results that J=2 gives good results for 161 ROIs and J=3 gives good results for 81 ROIs. The J value depends upon the size of calcifications.

Results

The abnormal ROIs of the mammogram are identified by bandfrequency based histogram technique. Figure 9(a) shows a 128×128 pixels abnormal ROI, Fig. 9(b–d) shows the binary responses are obtained by Hessian matrix and Fig. 9(e–g) shows the thresholded images are obtained by foveal segmentation method. Figure 9(h–j) shows the image responses obtained according to Eq. (14) and a final resultant image obtained according to Eq. (15) as shown in Fig. 9(k). In Fig. 9(l), the microcalcification clusters are indicated on the mammogram image.

We have tested our proposed algorithm in the suspected region (a region which does not contain calcifications, but it is marked as suspicious region by bandfrequency based histogram technique) as shown in Fig. 10(a). The final resultant image (Fig. 10(k)) contains no information, so the proposed approach based on eigenvalues of the Hessian matrix and foveal segmentation can efficiently detect the microcalcification clusters.

The Free-Response Operating Characteristic (FROC) curve is used to evaluate the performance of microcalcification detection methods. This plot provides true-positive detection ratio (TP) versus the average number of false positives (FPs) per image. The TP ratio refers to the percentage of microcalcifications that are truly detected and FP numbers/image refers to normal regions that are wrongly marked as abnormality by the proposed algorithm. We performed FROC analysis for 335 images that contained 242 microcalcification clusters, of which 237 clusters were detected correctly and 5 clusters were missed due to dense background. From 335 images (abnormal and normal images) out of 236 normal regions were mistakenly marked as suspicious regions. Hence, true positive rate $\left(\frac{Total\ number\ of\ TPs}{Total\ number\ of\ clusters}\right)$ of our CAD system is

Table 3 Comparison of TPs and FPs of various detection methods

References	Number of images (abnormal+normal images)	Number of clusters	Number of TPs	Number of FPs	True positive ratio with FP/image
Wang et al. [8]	370	269	218	352	81.04 % with 0.95 FPs
Hu et al. [21]	370	269	252	307	93.68 % with 0.83 FPs
Linguraru et al. [25]	370	269	257	271	95.53 % with 0.73 FPs
Mohanalin et al. [27]	370	269	260	249	96.65 % with 0.67 FPs
Proposed approach	370	269	263	254	97.76 % with 0.68 FPs

The clusters were obtained from MIAS, UCSF, and DDSM database with resolution of 50 and 42 μm/pixel

97.93 % (237/242) with a false positive rate of 0.704 (236/335). Table 1 shows the number of TPs and FPs detected by the proposed method.

We performed a comparison of our algorithm with the detection algorithm that was proposed by Mohanalin et al. [27] and Hu et al. [21]. Mohanalin et al. employed iterative thresholding technique by using Tsallis entropy and type II fuzzy index. They have used a type II fuzzy set for optimal thresholding. Hu et al. used a combination of a coarse segmentation and a fine segmentation, to segment suspicious lesions in multiscale analysis. The global threshold was selected from the derivative Probability Density Function of the image and it is utilized to segment the bright objects in the mammogram. Later, they have used window based adaptive thresholding to produce precise segmentation results. But both algorithms failed to segment various sizes of microcalcifications. We compared three algorithms by conducting FROC analysis for 335 images of 50 um/pixel resolution that contained 242 microcalcification clusters, of which 237 clusters were detected by the proposed method, 235 clusters were detected by Tsallis entropy method and 229 clusters were detected by Kai Hu method. The number of false positives obtained by proposed method, Tsallis entropy, and Kai Hu method were 236, 231, and 282. Therefore, the proposed method has the TP ratio of 97.93 % (237/242) with 0.70 (236/335) Fps per image, Tsallis entropy method has TP ratio of 97.11 % (235/242) with 0.69 (231/335) Fps per image, and Kai Hu method has TP ratio of 94.62 % (229/242) with 0.84 (282/335) Fps per image. Figure 11 demonstrates the superiority of our algorithm using FROC curve.

We used a small set of images obtained from another DDSM database from the local cancer institute consisting of 35 images with a resolution of 42 μm/pixel for comparison. In this collection, 24 images are abnormal images and 11 images are normal. Twenty-four mammograms contained one or more microcalcification clusters, which were annotated by a radiologist. The total number of microcalcification clusters was 27 (3 malignant lesions and 24 benign lesions). Out of 27 clusters, 26 clusters were detected correctly and 18 normal regions were mistaken for abnormal ones by the proposed method. The TP ratio of the proposed algorithm is 96.29 % (26/27) with the number of false positives per image is 0.51 (18/35). The Tsallis entropy method achieves TP ratio of 92.59 % (25/27) with 0.51 (18/35) FPs and Kai Hu method achieves TP ratio of 85.18 % (23/27) with 0.71 (25/35) FPs per image. The FROC curve for this comparison is shown in Fig. 12. The top line in the curve clearly indicates that the detection performance of the proposed algorithm is superior to conventional algorithms at different resolution of images. We analyzed our proposed approach with various detection methods in connection with the labeling of an experienced radiologist. Tables 2 and 3 summarize the performance of the proposed approach with existing algorithms.

Discussion and Conclusion

In this paper, we have developed a CAD scheme to assist the radiologists for accurate microcalcification clusters detection in digital mammography. The proposed approach is efficient for detecting clusters of various dimensions. The proposed algorithm operates in several stages. First, the suspicious regions in the digitized mammogram are detected by bandfrequency based histogram technique. The 128× 128 pixels square regions have been selected as abnormal ROIs from the mammogram. Then the insignificant high frequency noise in the abnormal ROIs is suppressed by traditional wavelet denoising scheme. We have designed a filter bank based on the Hessian matrix for computing second order partial derivatives of a mammogram image. The microcalcification structure is classified based on the eigenvalues of the Hessian matrix and the potential microcalcification pixels are distinguished against their background by adaptive thresholding technique (foveal) in the multiscale analysis. Finally, the microcalcifications are detected by a combination of the two methods. The proposed method achieves TP ratio of 97.76 % with 0.68 FPs. The strength of the proposed approach is that it detects various sizes of microcalcification clusters accurately by using multiscale filter without affecting their shapes. The limitation of our approach is that it failed to detect clusters accurately in dense mammogram especially in young women breast tissues. The normal tissues which appear as localized bright spots and nodular in structure are also detected by our computerized scheme. The ultimate goal of any CAD system is to reduce false positives in the detection process. In future, our study will focus on the texture features of microcalcification clusters to find out a better way to reduce false positives. The stage explains the extent of the cancer in the breast areas and it is based on the size of microcalcifications. It is an important factor to determine the treatment to be given to the patients. The number of the eigenvalues (λ_1, λ_2) of Hessian matrix less than zero are increased when the size of the microcalcification is increased. The work which is currently under development is aimed to compute the size of each microcalcification to assist clinical diagnosis.

References

1. http://www.breastcancer.org. Accessed 27 December 2011.
2. Heath M, Bowyer K, Kopans D, Moore R, Kegelmeyer P: "The digital database for screening mammography" In: Proceedings of the 5th International Workshop on Digital Mammography. Med Phys 662–671, 2000
3. Burhenne H, Burhenne L, Goldberg F, Hislop T, Worth AJ, Rebbeck PM, Kan L: Interval breast cancers in the screening mammography program of British Columbia: Analysis and classification. Am J Roentgenol 162:1067–1071, 1994

4. Bird RG, Wallace TW, Yankaskas BC: Analysis of cancers missed at screening mammography. Radiology 184:613–617, 1992
5. Cheng H-D, Lui YM , Freimanis RI: "A novel approach to microcalcification detection using fuzzy logic technique", IEEE Trans Med Imaging 17, no. 3, June 1998
6. Fogel DB, Wasson EC, Boughton EM, Porto VW: Evolving artificial neural networks for screening features from mammograms. Artif Intell Med 14:317–326, 1998
7. Jiang J, Yao B, Wason AM: A genetic algorithm design for microcalcification detection and classification in digital mammograms. Comput Med Imaging Graph 31(no.1):49–56, 2007. Jan
8. Wang TC, Karayiannis NB: "Detection of microcalcifications in digital mammograms using wavelets", IEEE Trans Med Imaging 17, no. 4, August 1998
9. Mencattini A, Salmeri M, Lojacono R, Frigerio M, Caselli F: Mammographic images enhancement and denoising for breast cancer detection using dyadic wavelet processing. IEEE Trans Instrum Meas 57(7):1422–1430, 2008. July
10. Naveed N, Choi T-S, Jaffar A: Malignancy and abnormality detection of mammograms using DWT features and ensembling of classifiers. Int J Phys Sci 6(8):2107–2116, 2011. April
11. Nakayama R, Uchiyama Y, Yamamoto K, Watanabe R, Namba K: Computer-aided diagnosis scheme using a filter bank for detection of microcalcification clusters in mammograms. IEEE Trans Biomed Eng 53(2):273–283, 2006. Feb
12. Frangi A, Niessen W, Vincken K, Viergever M: Multiscale vessel enhancement filtering. Lect Notes Comput Sci 1496:130–137, 1998
13. Sato Y, Westin C, Bhalerao A, Nakajima S, Shiraga N, Tamura S, Kikinis R: Tissue classification based on 3-D local intensity structure for volume rendering. IEEE Trans Vis Comput Graph 6(no. 2):160–180, 2000. Apr./Jun
14. Zhou C, Chan HP, Shahiner B, Hadjiiski LM, Chughtai A, Patel S, Wei J, Ge J, Cascade PN, Kazerooni EA: Automatic multiscale enhancement and segmentation of pulmonary vessels in CT pulmonary angiography images for CAD applications. Med Phys 34 (12):4567–4577, 2007
15. Panayiotis DK, Cristina K, Anna NK, Alexandra DK, Lena IC: Vessel tree segmentation in presence of interstitial lung disease in MDCT. IEEE Trans Inform Technol Biomed 15, no.2, March 2011
16. Yu Y, Zhao H: "Enhancement filter for computer-aided detection of pulmonary nodules on thoracic CT images", in proc. 6th International Conference on Intelligent Systems Design and Applications, 2006
17. Agam G, Armato III, SG, Wu C: Vessel tree reconstruction in thoracic CT scans with application to nodule detection. IEEE Trans Med Image 24(4):486–499, 2005
18. Kom G, Tiedeu A, Kom M: Automated detection of masses in mammograms by local adaptive thresholding. Comput Biol Med 37(1):37–48, 2007. Jan
19. Zhang XP, Desai MD: Segmentation of bright targets using wavelets and adaptive thresholding. IEEE Trans Image Process 10 (7):1020–1030, 2001. July
20. Sahba, F, Venetsanopoulos A: "A new method for the detection of microcalcification in mammograms", International conference on information technology and applications in Biomedicine, cyprus, Nov. 2009
21. Hu K, Gao X, Li F: "Detection of suspicious lesions by adaptive thresholding based on multiresolution analysis in mammograms" IEEE Trans Instrum Meas 60, no. 2, Feb. 2011
22. Xu Y, Weaver JB, Healy Jr, DM, Lu J: Wavelet transform domain filters: a spatially selective noise filtration technique. IEEE Trans Image Process 3:747–758, 1994. Nov
23. Donoho DL, Johnstone IM: Ideal spatial adaptation via wavelet shrinkage. Biometrika 81:425–455, 1994
24. Yoshinobu S, et al.: "3D multi-scale line filter for segmentation and visualization of curvilinear structures in medical images", in proc. of the First joint conference on computer vision, virtual reality and robotics in medicine and medial robotics and computer-assisted surgery, vol. 1205 of Lecture Notes in Computer Science, pages 213–222, March 1997
25. Linguraru MG, Marias K, English R, Brady M: A biologically inspired algorithm for microcalcification cluster detection. Med Image Anal 10(no. 6):850–862, 2006. Dec
26. Oh W-V, Kim KG, Kim Y-J, Kang HS, Ro JS, Moon WK: Detection of microcalcifications in digital mammograms using foveal method. J Korean Soc Med Inform 15:165–172, 2009
27. Beenamol M, Kalra PK, Kumar N: A novel automatic microcalcification detection technique using Tsallis entropy & a type II fuzzy index. Comput Math Appl 60:2426–2432, 2010. Oct